Improved arrayed-waveguide-grating layout avoiding systematic phase errors

Nur Ismail,* Fei Sun, Gabriel Sengo, Kerstin Wörhoff, Alfred Driessen, René M. de Ridder, and Markus Pollnau

Integrated Optical MicroSystems Group, MESA + Institute for Nanotechnology, University of Twente, P.O. Box 217, 7500 AE Enschede, The Netherlands
**n.ismail@ewi.utwente.nl*

Abstract: We present a detailed description of an improved arrayed-waveguide-grating (AWG) layout for both, low and high diffraction orders. The novel layout presents identical bends across the entire array; in this way systematic phase errors arising from different bends that are inherent to conventional AWG designs are completely eliminated. In addition, for high-order AWGs our design results in more than 50% reduction of the occupied area on the wafer. We present an experimental characterization of a low-order device fabricated according to this geometry. The device has a resolution of 5.5 nm, low intrinsic losses (< 2 dB) in the wavelength region of interest for the application, and is polarization insensitive over a wide spectral range of 215 nm.

OCIS codes: (130.7408) Wavelength filtering devices; (300.6190) Spectrometers.

References and links

1. M. K. Smit, "New focusing and dispersive planar component based on an optical phased array," Electron. Lett. **24**(7), 385–386 (1988).
2. H. Takahashi, S. Suzuki, K. Kato, and I. Nishi, "Arrayed-waveguide grating for wavelength division multi/demultiplexer with nanometer resolution," Electron. Lett. **26**(2), 87–88 (1990).
3. C. Dragone, "An N x N optical multiplexer using a planar arrangement of two star couplers," IEEE Photon. Technol. Lett. **3**(9), 812–815 (1991).
4. N. Ismail, B. I. Akca, F. Sun, K. Wörhoff, R. M. de Ridder, M. Pollnau, and A. Driessen, "Integrated approach to laser delivery and confocal signal detection," Opt. Lett. **35**(16), 2741–2743 (2010).
5. M. C. Hutley, *Diffraction Gratings* (Academic, 1982).
6. C. D. Lee, W. Chen, Q. Wang, Y.-J. Chen, W. T. Beard, D. Stone, R. F. Smith, R. Mincher, and I. R. Stewart, "The role of photomask resolution on the performance of arrayed-waveguide grating devices," J. Lightwave Technol. **19**(11), 1726–1733 (2001).
7. T. Goh, S. Suzuki, and A. Sugita, "Estimation of waveguide phase error in silica-based waveguides," J. Lightwave Technol. **15**(11), 2107–2113 (1997).
8. R. Adar, C. H. Henry, C. Dragone, R. C. Kistler, and M. A. Milbrodt, "Broad-band array multiplexers made with silica waveguides on silicon," J. Lightwave Technol. **11**(2), 212–219 (1993).
9. M. K. Smit and C. Van Dam, "PHASAR-based WDM-devices: Principles, design and applications," IEEE J. Sel. Top. Quantum Electron. **2**(2), 236–250 (1996).
10. F. M. Soares, W. Jiang, N. K. Fontaine, S. W. Seo, J. H. Baek, R. G. Broeke, J. Cao, K. Okamoto, F. Olsson, S. Lourdudoss, and S. J. B. Yoo, "InP-based arrayed-waveguide grating with a channel spacing of 10 GHz," in *Proceedings of the National Fiber Optic Engineers Conference* (Optical Society of America, Washington DC, 2008), paper JThA23.
11. R. N. Sheehan, S. Horne, and F. H. Peters, "The design of low-loss curved waveguides," Opt. Quantum Electron. **40**(14-15), 1211–1218 (2008).
12. K. Takada, M. Abe, T. Shibata, and K. Okamoto, "1-GHz-spaced 16-channel arrayed-waveguide grating for a wavelength reference standard in DWDM network systems," J. Lightwave Technol. **20**(5), 850–853 (2002).
13. P. J. Caspers, G. W. Lucassen, E. A. Carter, H. A. Bruining, and G. J. Puppels, "In vivo confocal Raman microspectroscopy of the skin: noninvasive determination of molecular concentration profiles," J. Invest. Dermatol. **116**(3), 434–442 (2001).
14. K. Wörhoff, C. G. H. Roeloffzen, R. M. de Ridder, A. Driessen, and P. V. Lambeck, "Design and application of compact and highly tolerant polarization independent waveguides," J. Lightwave Technol. **25**(5), 1276–1283 (2007).

#142949 - $15.00 USD Received 18 Feb 2011; revised 15 Apr 2011; accepted 17 Apr 2011; published 20 Apr 2011

1. Introduction

The arrayed-waveguide grating (AWG) was first proposed by Smit in 1988 [1] and subsequently reported by Takahashi *et al.* in 1990 [2] and Dragone in 1991 [3]. Since then it has developed into one of the most important devices in integrated optics. Its imaging [4] and dispersive properties make it an ideal device for wavelength separation in wavelength-division-multiplexing and spectroscopic applications. The working principle of the AWG is briefly described referring to Fig. 1(a).

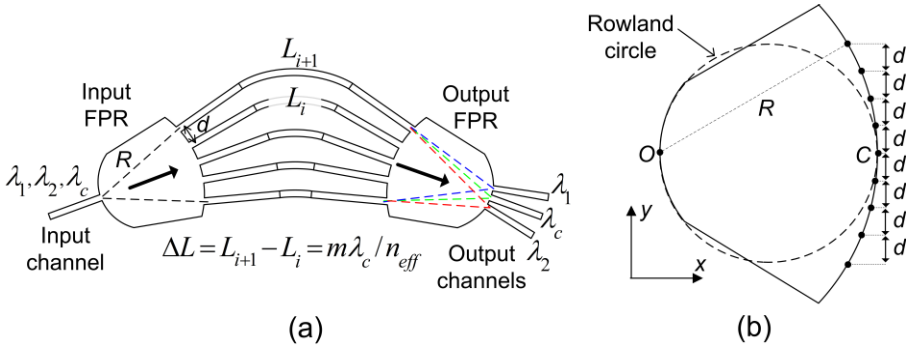

Fig. 1. (Color online) (a) Schematic layout of an AWG and (b) schematic of a Rowland grating mounting where the dots indicate the positions of the arrayed waveguides arranged such that the chords have equal projections on the y axis.

Light from an input channel waveguide is guided to a free-propagation region (FPR) where it diffracts in the horizontal direction and is coupled to an array of channel waveguides which are arranged on a circle of radius R (grating line) equal to the length of the FPR. On this circle the arrayed waveguides are spaced by a center-to-center distance $d << R$. Due to the limited number of arrayed waveguides, part of the light is lost to the sides of the array (spillover losses). This arrangement, comprising the input channel, the FPR, and the array of collecting waveguides forms a $1 \times N$ star coupler which couples the light from one input waveguide into N arrayed waveguides. The arrayed waveguides have a linearly increasing length, and the length difference between adjacent waveguides is $\Delta L = m\lambda_c/n_{eff}$, where m is an integer, λ_c is the central wavelength of the AWG, and n_{eff} is the effective refractive index of the arrayed waveguides at the central wavelength. Light exiting from the array enters a second FPR where the output terminations of the arrayed waveguides are again arranged on a circle with radius R (as for the input FPR). The center of this circle coincides with the entrance facet of the central output channel of the AWG. With this arrangement, when light at wavelength λ_c is sent through the input channel, a circular wave front is generated at the output of the array, and the light is focused into the central output channel. For light at a different wavelength ($\lambda \neq \lambda_c$) the circular wave front generated at the output is tilted with respect to the one for λ_c, and the focal spot is located at a different spatial position. Output channels can be placed at different positions at the output of the second FPR to collect individual spectral components of the input signal. The design just described makes use of a constant angular spacing between the arrayed waveguides. An alternative approach, which has the advantage of reduced aberrations is the Rowland mounting [5] where the arrayed waveguides, instead of being positioned at a constant angular spacing, are positioned such that chords (or center to center distances) have a constant projection on the y axis, as shown in Fig. 1(b). In this type of mounting the input and output channels are positioned on a circle (Rowland circle) and point towards the center C of the grating line. The Rowland circle has a radius of $R/2$ and is tangent to the grating line in C.

A typical cause of degradation in the response of an AWG is the presence of phase errors across the arrayed waveguides; these can be regarded as deviations of the optical path lengths from the designed values and can be divided into two categories. The first category comprises phase errors that arise from the device fabrication process; these phase errors are caused by

#142949 - $15.00 USD Received 18 Feb 2011; revised 15 Apr 2011; accepted 17 Apr 2011; published 20 Apr 2011

random variations in the waveguide width, which depend on the resolution of the mask used in the photolithographic process [6], as well as waveguide side-wall roughness and non-uniformities of the guiding layer properties, such as its refractive index and thickness [7]. The second category includes systematic phase errors due to the design of differently bent sections in the arrayed waveguides. In each bend light experiences an effective refractive index which is a function of the bending radius. Usually, the difference between the effective indices in the straight and bent sections of an arrayed waveguide is very small (between 1×10^{-5} and 1×10^{-4}); however, when the arrayed waveguide bends over a large angle (i.e. $\sim\pi$) and has a small bending radius, the induced phase deviation from the designed value may become significant. In particular, in conventional AWG layouts, such as horseshoe and s-shaped AWGs [8,9] in which the bends in the arrayed waveguides all differ in radius and length, the changes in the optical path length are different from waveguide to waveguide within the array, leading to a distortion of the wave fronts in the second FPR with a consequent defocusing effect.

Systematic phase errors are predictable and can, therefore, be accounted for when designing the relative delays between adjacent arrayed waveguides. However, this requires numerical simulations and may not lead to perfect cancellation of these phase errors due to both, simulation inaccuracies and fabrication tolerances. The AWG introduced by Takahashi *et al.* [2] consisted of identical bends (four 90° bends in each arrayed waveguide), however the input and output sections of the arrayed waveguides were parallel to each other and not arranged on a star coupler. The use of star couplers in AWGs was first proposed by Dragone in 1991, in which two star couplers were interconnected by arrayed waveguides of unequal lengths and with a fixed angular separation [3]. In the star-coupler configuration the non-zero angle between adjacent waveguides of the array makes it difficult to use identical bends in the AWG layout. A partial solution to the problem was proposed in Ref. 10, where only bends with equal bending radius were used in the arrayed waveguides. This, however, did not completely cancel the systematic phase errors, since the lengths of the bends were not equal across the array.

In this work we propose a new layout in which all the arrayed waveguides have identical bends. Our design is based on arranging the arrayed waveguides with a constant angular spacing, in this way deviating from the Rowland mounting although the input and output channels are still positioned on the Rowland circle. This deviation, in terms of position of the arrayed waveguides, is in general very small: as will be shown in section 4. In our fabricated device the positions of the arrayed waveguides deviate with respect to the Rowland mounting by 165 nm maximum, which is less than the resolution of the e-beam mask used in the fabrication. In sections 2 and 3, we show that the identical bend layout can be used for both, low-order and high-order AWG designs; besides eliminating the systematic phase errors, in the case of high-order AWGs this layout presents the additional advantage of reduced area compared to the conventional horse-shoe layout. In section 4 we present experimental results on the characterization of a broadband AWG which makes use of the novel design. This AWG, which is designed for a specific application, has a resolution of 5.5 nm and a polarization-independent response over a very large spectral range of 215 nm (the maximum observed shift between the responses for the two polarizations is a factor of 10 smaller than the resolution).

2. The identical-bend design

As a starting point we considered the broadband anti-symmetric AWG model introduced by Adar et al. [8]. The geometry is shown in Fig. 2.

#142949 - $15.00 USD Received 18 Feb 2011; revised 15 Apr 2011; accepted 17 Apr 2011; published 20 Apr 2011

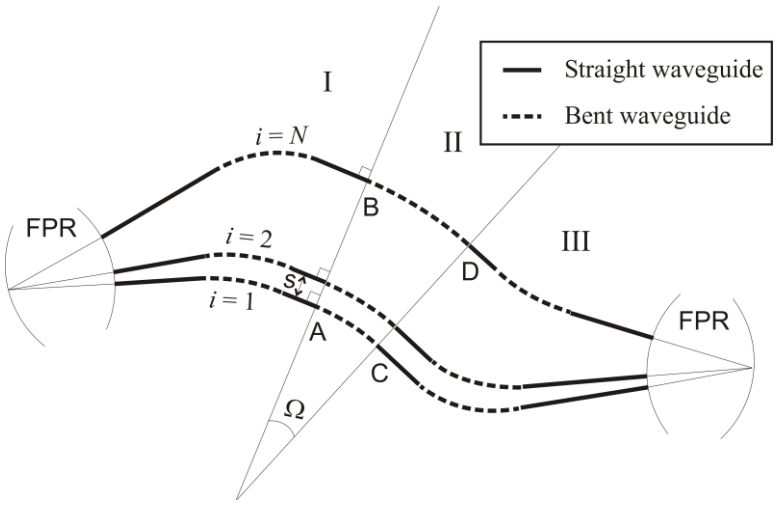

Fig. 2. Anti-symmetric layout of a conventional broadband arrayed waveguide grating having *N* arrayed waveguides. The free-propagation-regions (FPRs) are indicated schematically.

In this model each waveguide is composed of four straight sections interconnected by three arcs. The layout can be divided into three parts; parts I and III are identical but rotated by an angle $\pi + \Omega$. In part I each arrayed waveguide is bent to normal incidence on line $\overline{AB}$. Two conditions are imposed on the model for the waveguides of part I: firstly, the separation *s* between adjacent waveguides on line $\overline{AB}$ is constant; secondly, the length of each waveguide is increased with respect to that of the previous waveguide by a constant amount. In this way, if part I is directly connected with part III, all waveguides will necessarily have the same length. The length difference between the arrayed waveguides is introduced by the arcs of the interposed part (part II). A more detailed description can be found in [8].

Smaller size of the AWG can be achieved with smaller bending radii; yet, particular care must be taken to keep the waveguide bend losses at an acceptable level. Low-loss curved waveguides can be achieved by introducing non-linear curvatures [11]. However, if all the arrayed waveguides exhibit different nonlinear bends, the phase errors introduced by small bending radii can reach significant levels. As explained in the next section, in high-order conventional AWGs there is a trade-off between device size, losses, and systematic phase errors, which is a key motivation for developing a layout that intrinsically avoids the latter. Introducing the length differences only in the straight sections of the arrayed waveguides would allow one to design bends with any desired shape without introducing systematic phase errors to the AWG, because the same bend is used in all arrayed waveguides.

We have implemented an AWG layout in which all the waveguides make use of identical bends, while the length difference ΔL between adjacent waveguides is obtained in the straight waveguide sections. Our layout is inspired by Adar's work [8], with the main difference that for low-order designs we do not use a central part to introduce the length differences (a central part will be reintroduced for high-order designs, as discussed later); instead, we only use two parts which are shown in Fig. 3. A prime is used to distinguish the quantities of the right half, see Fig. 3(b), from those of the left half, see Fig. 3(a).

#142949 - $15.00 USD Received 18 Feb 2011; revised 15 Apr 2011; accepted 17 Apr 2011; published 20 Apr 2011

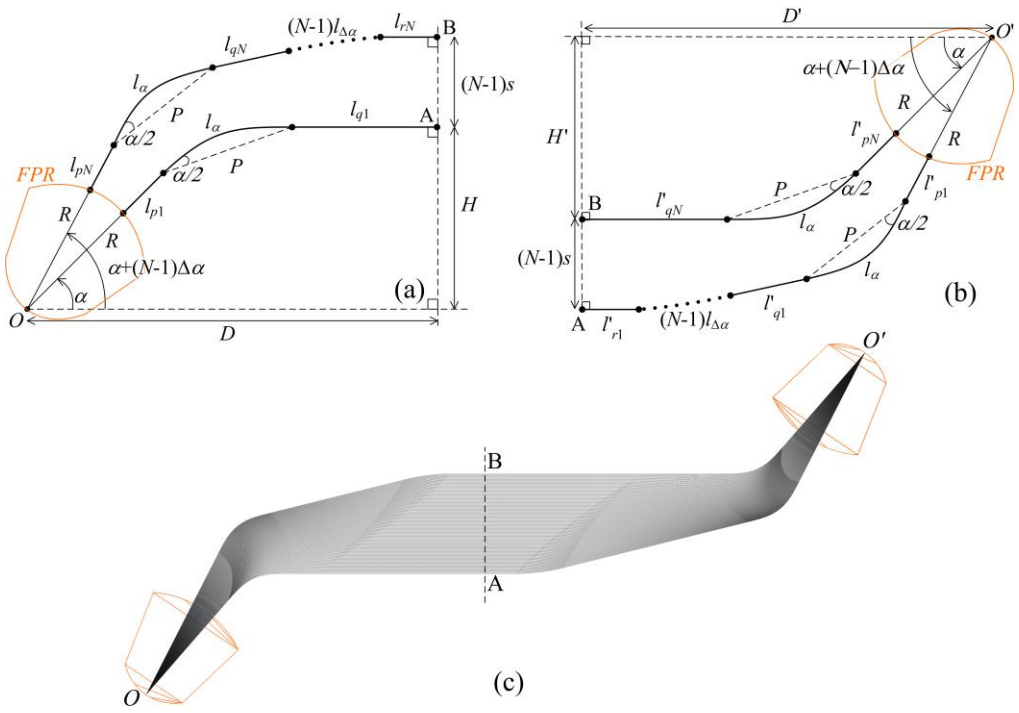

Fig. 3. (Color online) (a) Left half and (b) right half of the identical-bend AWG layout, where waveguides are indicated using a bold line; (c) schematic of the complete layout in which both halves are interconnected.

For both halves we impose that the separation s between two adjacent waveguides on line $\overline{\mathrm{AB}}$ is constant. However, for the left half we impose that the length of each waveguide is increased with respect to the length of the previous waveguide by the amount $l_i - l_{i-1} = a + \Delta L/2$, where a is an arbitrary constant; in contrast, for the right half, we impose that $l'_i - l'_{i-1} = \Delta L/2 - a$. When both halves are connected to each other, the length difference between adjacent arrayed waveguides will be ΔL. Our layout, for grating orders $m > 0$, is not anti-symmetric, which is different from Adar's design.

In Fig. 3(a) we present a schematic of the left half of the AWG. R is the radius of the FPR and N is the total number of arrayed waveguides. For clarity, only the first waveguide ($i = 1$), which we will refer to as the 'reference waveguide', and the last waveguide ($i = N$) are shown. The angle between any two adjacent waveguides of the array is $\Delta\alpha$, while the angle that the reference waveguide makes with the horizontal axis is indicated by α. The device makes use of only two types of bends: type 1 bends by an angle α, while type 2 bends by $\Delta\alpha$. These bends are the building blocks to be used in equal numbers in all the arrayed waveguides. As shown in Fig. 3(a), all waveguides are bent to normal incidence on line $\overline{\mathrm{AB}}$. This means that the waveguide with $i = 1$ is bent by an angle α, the waveguide with $i = 2$ by $\alpha + \Delta\alpha$, and so on. The i^{th} waveguide, which is bent by $\alpha + (i - 1)\,\Delta\alpha$, has one bend of type 1 and $i - 1$ bends of type 2.

Figure 3(b) displays a schematic of the right half of the AWG. The waveguides are numbered in the same order as on the left half; the lowest waveguide is number 1 and will be connected to waveguide number 1 of the left half; the uppermost waveguide is number N and will be connected to waveguide number N of the left half. On the right half, waveguide N includes one bend of type 1, waveguide $N - 1$ has one bend of type 1 and one bend of type 2, and so on. When we connect all the waveguides of the left half with those of the right half, each arrayed waveguide i has the same number of bends, namely two bends of type 1 and $N - 1$ bends of type 2. Consequently, any bend type (e.g. constant bend, linear bend, nonlinear

#142949 - $15.00 USD Received 18 Feb 2011; revised 15 Apr 2011; accepted 17 Apr 2011; published 20 Apr 2011

bend) and length can be chosen. Nevertheless, it is preferable to find a good compromise between the length of a bend and its bending radius to reduce propagation losses as well as the size of the device. For example, the bend of type 2, which is repeated $N - 1$ times in each waveguide, has typically a very small length (on the order of 10–20 μm), since the angle $\Delta\alpha$ is typically very small ($\Delta\alpha = d / R \sim 10^{-3}$ rad, see Fig. 1). For this reason, a small bending radius can be used if the number of waveguides N is small, while a larger minimum bending radius is preferable in case of large N, i.e., when many bends of type 2 are connected to each other in sequence. For the bends of type 2, circular bends can avoid bend-to-bend transition losses and undesirable periodicity in each waveguide (as would be the case when connecting many nonlinear bends to each other), whereas nonlinear bends can eliminate the straight-to-bend transition losses introduced by circular bends. Furthermore, in high-index-contrast waveguide systems, an offset is usually required when interconnecting straight and bent waveguides to reduce the mode mismatch at the junction. In this case the proposed AWG geometry gives more flexibility in the design without leading to a higher design complexity than when using the conventional geometry. For example, while the conventional S-shaped AWG has six straight-to-bend interfaces requiring the offset, the proposed AWG only requires four offsets, since the bends of type 1 can be non-linear bends with a gradual straight-to-bend transition. The details of the geometry are discussed in the Appendix. In Fig. 3(c) we present, for clarity, the complete layout of the AWG.

3. Design and simulation of high-order AWGs with the identical-bend layout

As previously anticipated, the proposed identical-bend layout can also be used to design high-order AWGs. Generally, with increasing order of the AWG the device becomes larger; for very high orders the phase errors, in particular those arising from fabrication non-uniformities, may become so significant (tens of radians) that a procedure of photosensitive phase compensation is necessary after device fabrication [12]. To limit these phase errors the device size must be reduced; this is done by choosing a smaller value for the minimum bending radius, which, on the other hand, results in increased losses and increased systematic phase errors in a conventional AWG. In contrast, in the case of an identical-bend AWG it results only in an increase of the losses.

As shown in Fig. 4, the design of a high-order AWG using the identical-bend layout is performed by simply interconnecting the two parts that have been described in the preceding section through an intermediate part, in order to introduce the necessary length differences. The i^{th} waveguide of the intermediate part, which is connected to the i^{th} waveguides of both, left and right halves, is composed of two equal straight sections, with a length given by $(i - 1)\Delta L/2$, interconnected by a curve with an angle $\varphi = 2\arctan(\Delta L/2s)$ which is repeated in all waveguides. In this way, the lengths of the waveguides of the left and right parts can even be designed by imposing $m = 0$, so that they do not contribute to the path length differences which, in this case, are introduced only by the central part. This design differs from Adar's design only by the fact that it makes use of identical bends. If desired, it is also possible to distribute the length differences over both, the lateral and central parts.

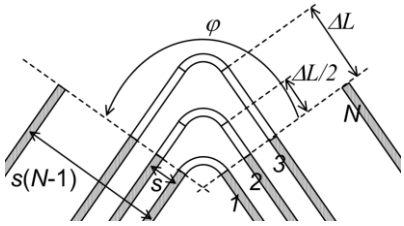

Fig. 4. Interconnection between the left and right halves of the AWG for high-order designs. The terminal parts of the waveguides of the left and right halves are shown in gray, and are numbered from 1 to N.

#142949 - $15.00 USD Received 18 Feb 2011; revised 15 Apr 2011; accepted 17 Apr 2011; published 20 Apr 2011

One of the advantages of the identical-bend high-order layout over the conventional layout is that it can lead to a device with a smaller footprint. We illustrate this fact by comparing two designs of the same AWG, one making use of the identical-bend geometry and the other of the conventional geometry. For the design we chose waveguides with the same cross-section and refractive-index contrast as those described in the next section. The following parameters were chosen for the AWG: central wavelength λ_c = 881.53 nm, wavelength spacing between the output channels $\Delta\lambda$ = 0.01 nm, order m = 5877, minimum bending radius r_{min} = 1700 μm, FPR radius R = 1126 μm, separation between the arrayed waveguides at the FPR d = 7.5 μm, and N = 31 arrayed waveguides. The minimum bending radius was chosen to have negligible bending losses (below 2×10^{-4} dB/cm) when taking into account the fabrication tolerances. For both layouts we optimized the geometrical parameters to obtain compact footprints. By calculating the area of the two designs (excluding the input and output channels) we obtain approximately 5.4 cm^2 for the conventional layout and 3.4 cm^2 for the identical-bend layout (an area reduction of 37%). Despite the reduction in area, the identical-bend design suffers from being longer than the conventional design. The length difference in the analyzed case (with 31 arrayed waveguides) is only of a few millimeters, but increases linearly with the number of waveguides.

If the device size is reduced by use of smaller bending radii at the expense of increased losses, the identical-bend design does not incur the systematic phase errors that degrade the performance in the conventional design. In case the minimum bending radius is reduced to 850 μm, we obtain 4.5 cm^2 area for the conventional design and 2.1 cm^2 for the identical-bend design, corresponding to a reduction of the occupied area of 54% (see Fig. 5). In this case the bending losses (calculated accounting for fabrication tolerances) are around 0.3 dB/cm, resulting in a total bending loss lower than 0.1 dB for the entire device. We simulated the effect of the systematic phase errors on these AWGs. Figure 6(a) shows a comparison between the identical-bend design, in which the systematic phase errors are not present, and the conventional design. The phase errors in the conventional design produce a shift in the central wavelength of the channels (approximately 0.002 nm), and a deformation in the passband shape. In Fig. 6(b) we overlapped the response of one output channel of the identical-bend AWG with the response of the same output channel of the conventional AWG to show the effect of the phase errors on the passband shape. To better illustrate the difference in passbands the response of the conventional AWG was shifted by 0.002 nm such that the the centers of the two pass-bands coincide.

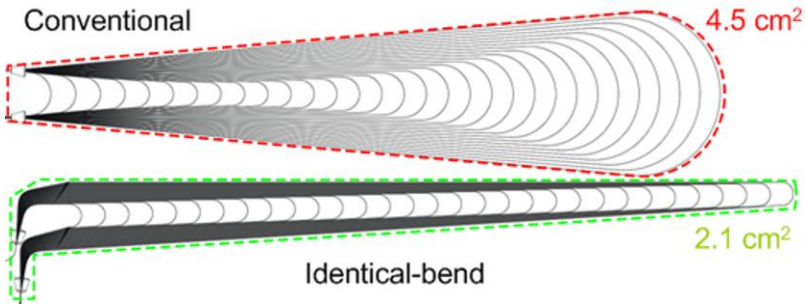

Fig. 5. (Color online) Comparison of the conventional and identical-bend layouts in terms of the occupied area.

#142949 - $15.00 USD Received 18 Feb 2011; revised 15 Apr 2011; accepted 17 Apr 2011; published 20 Apr 2011

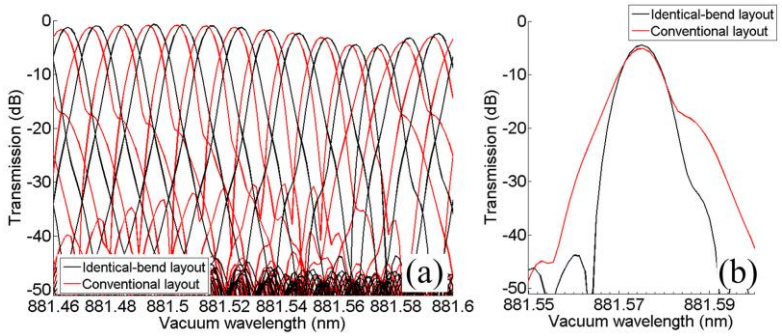

Fig. 6. (Color online) (a) Simulated effect of systematic phase errors on the response of an AWG designed with the conventional layout (red line). These phase errors are not present in the identical-bend layout (black line). Both graphs are for the transverse-electric (TE) polarization; (b) the response of an outer channel of the identical-bend AWG is overlapped with that of the same channel of the conventional AWG to show the difference in passband.

The systematic phase errors for the two conventional AWGs with r_{min} = 1700 μm and 850 μm, respectively, are displayed in Fig. 7. The systematic phase errors are considered as the deviations of the phase difference between each two adjacent arrayed waveguides with respect to the intended value of $2m\pi$ (at the central wavelength).

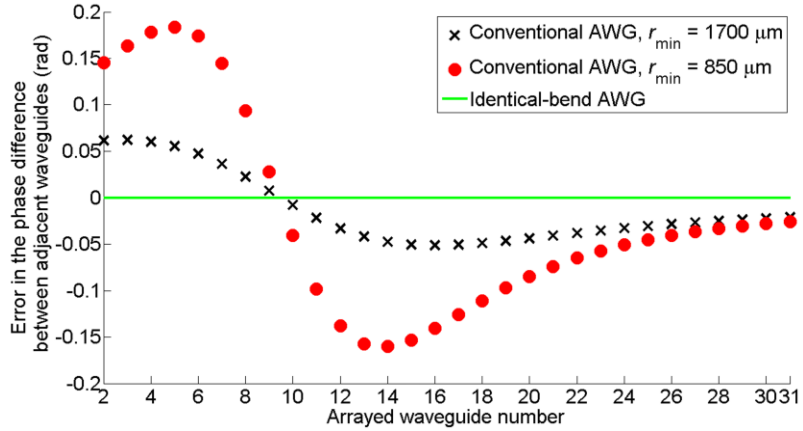

Fig. 7. (Color online) Calculated systematic phase errors between adjacent waveguides in a conventional AWG design for the transverse-electric (TE) polarization, and for two different values of the minimum bending radius r_{min}. These phase errors are not present in the identical-bend design, whatever value of the minimum bending radius is used (green line).

4. Experimental results on a broadband AWG design

In this section we present results of the experimental characterization of a broadband AWG that makes use of the simpler form of the identical-bend layout described in section 2.

Our experimental AWG device is designed for the analysis of Raman emission from human skin to determine its natural moisturizing factor (NMF) which is an important parameter in skin typing for the cosmetic industry [13]. With laser excitation at a wavelength of 785 nm and a Raman shift between 700 cm^{-1} and 1700 cm^{-1}, the wavelength range of interest is between 830 and 900 nm. The application requires polarization insensitivity, a central wavelength of the AWG of 881 nm (corresponding to the spectral position of one of the NMF bands to be detected), and a minimum resolution of 5.5 nm. Particular care must be taken to avoid overlap between the excitation wavelength – imaged at a higher order – and any of the output channels; in our particular case, this translates into the requirement of a minimum FSR greater than 115 nm. To fulfill all these requirements, we designed a 3rd-order

#142949 - $15.00 USD Received 18 Feb 2011; revised 15 Apr 2011; accepted 17 Apr 2011; published 20 Apr 2011

AWG using low-birefringence silicon oxynitride (SiON) channel waveguides with a SiO_2 cladding. The waveguides have core and cladding refractive indexes of 1.509 and 1.454, respectively, in transverse-electric (TE) polarization. The material birefringence, defined as the difference between the refractive indices for the transverse-magnetic (TM) and TE polarizations, of SiON and SiO_2 at 830 nm is $\Delta n_{\text{TM-TE}} = 2.1 \times 10^{-3}$ and 1.0×10^{-3} [14], respectively. The chosen waveguide geometry, a cross-section of 2 μm × 0.52 μm, results in low channel-waveguide birefringence ($\Delta n_{eff,\text{TM-TE}} < 5 \times 10^{-4}$) across the Raman band of interest. Although the birefringence in the bends has a slightly different value, this does not affect the response of the identical-bend AWG. When designing the AWG according to the proposed geometry, the angle $\alpha = 49°$ was chosen to minimize the size of the device, while $\Delta\alpha \cong 0.1°$ was fixed once the FPR length $R \cong 4$ mm and the separation $d = 7.5$ μm between the arrayed waveguides at the FPR interface were determined. The latter two parameters are related through the AWG design equations [9] to the output channel wavelength spacing $\Delta\lambda$, which in our case is 5.5 nm. Furthermore, we chose a relatively large number of arrayed waveguides ($N = 131$) as a compromise between minimizing the spillover losses and having a reduced overall device size. The bends used in our implementation are cosine bends, where the curvature changes continuously from a value of zero at the input and output ports, reaching a maximum in the center of the bend. The minimum bending radius for the type 1 bend was 1750 μm to guarantee bending losses below 0.1 dB/cm (calculated accounting for fabrication tolerances) at the highest wavelength in the spectral region of interest. This choice of bending radius resulted in a bend length of 2500 μm. Since the type 2 bend is repeated many times, the change in curvature across each interconnected bend translates into a periodicity of the effective index of the guided mode. Hence, for the bend of type 2, we chose a much larger minimum bending radius of 5100 μm to obtain a negligible change in the effective index ($\Delta n_{\text{eff}} \sim 2.1 \times 10^{-6}$) across the bend. This choice resulted in a bend length of 15 μm. The device was fabricated using an e-beam written mask having a minimum resolvable feature size of 0.7 μm, and a defect density of 0.64 defects/inch^2 with maximum defect size of 2 μm. As mentioned in the introduction, the design is based on an arrangement of the arrayed waveguides with a constant angular spacing. For this reason the condition of equal chord projections required by the Rowland mounting is not met. However, the maximum deviation of arrayed waveguide positions at the grating line from the Rowland mounting configuration is about 0.16 μm. Not only is this value much smaller than the e-beam mask resolution, it is also much smaller than the waveguide width. Therefore, in this case, our layout is a good approximation of the Rowland mounting geometry.

For device characterization we used the setup shown in Fig. 8. Light from a Fianium super-continuum source (from 400 nm to 1800 nm) was sent through a polarization beam splitter and a red-glass filter (RG715) to suppress the undesired region of the spectrum (400-715 nm). The light was then focused into the input waveguide of the AWG by a microscope objective with a numerical aperture (NA) of 0.65 and a magnification of × 40. The spectral response of the AWG was measured by coupling each output channel to a spectrometer (iHR550 Horiba) through a single-mode fiber. The input and output slit widths of the spectrometer were adjusted to the same value of 0.1 mm and the measurement resolution was 0.25 nm.

#142949 - $15.00 USD Received 18 Feb 2011; revised 15 Apr 2011; accepted 17 Apr 2011; published 20 Apr 2011

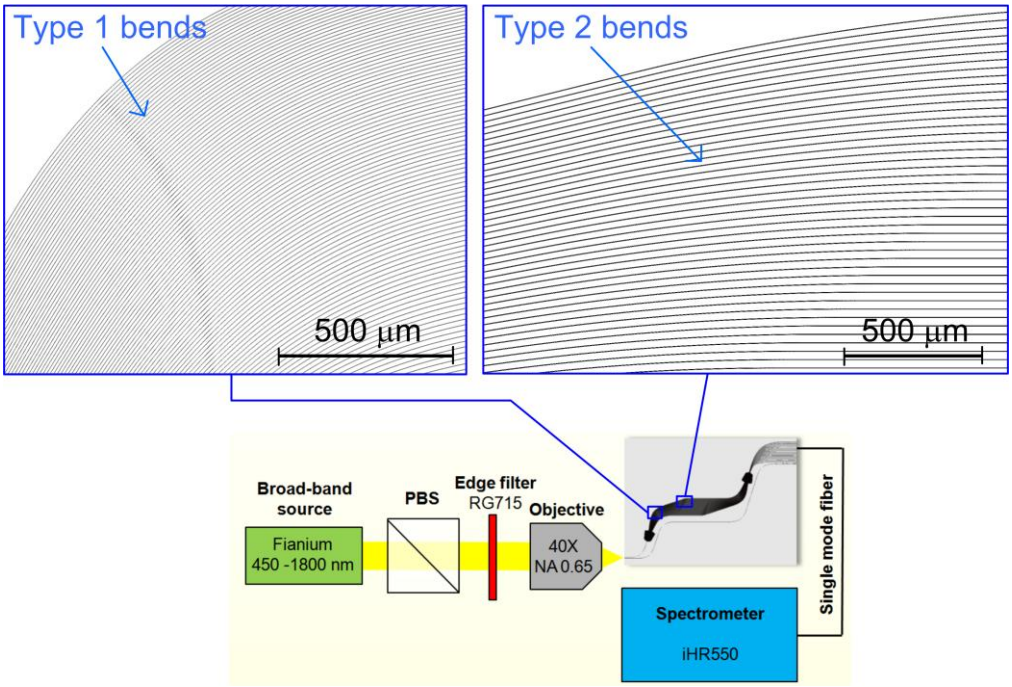

Fig. 8. (Color online) Setup used to characterize the AWG. PBS = polarizing beam splitter. In the insets we present two enlarged views of the AWG layout pointing at the locations of the bends of type 1 and 2.

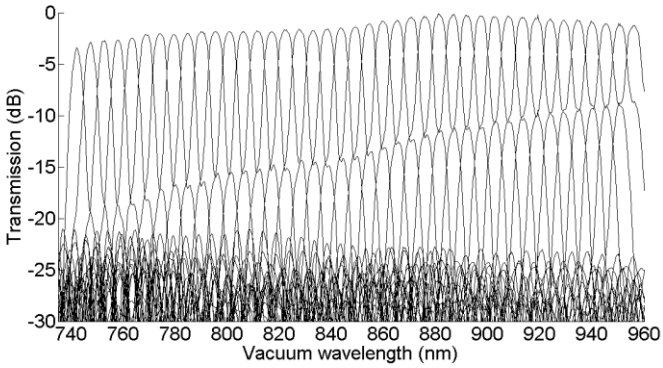

Fig. 9. Measured spectral response of the AWG for TE polarization.

The measured response was normalized with respect to the spectrum from a separate reference channel on the same chip and is shown for TE polarization in Fig. 9. As can be observed, the intrinsic losses (excluding coupling losses and propagation losses) of the AWG are very low, ranging from 1.1 dB for the central channel up to a maximum of 1.8 dB at the edges of the spectral region of interest (830 to 900 nm). We estimate an error in the measured loss value of ~2 dB since it is not possible to achieve the same coupling conditions in all the output channels as those for the reference waveguide. We also measured the total transmission through the device (from input fiber to output fiber) to be 9.6% at a wavelength of 832 nm. The fiber to chip coupling efficiency was estimated to be 70% per facet using mode overlap calculations; the remaining 40% loss is due to propagation losses.

Figure 10 displays the normalized responses for TE and TM polarizations measured for 5 central and 11 outer channels of the device. The measured FSR is 215 nm, and the device is

#142949 - $15.00 USD Received 18 Feb 2011; revised 15 Apr 2011; accepted 17 Apr 2011; published 20 Apr 2011

polarization insensitive over the whole spectral range, the maximum shift between TE and TM polarizations being 0.5 nm, which is more than 10 times smaller than the resolution.

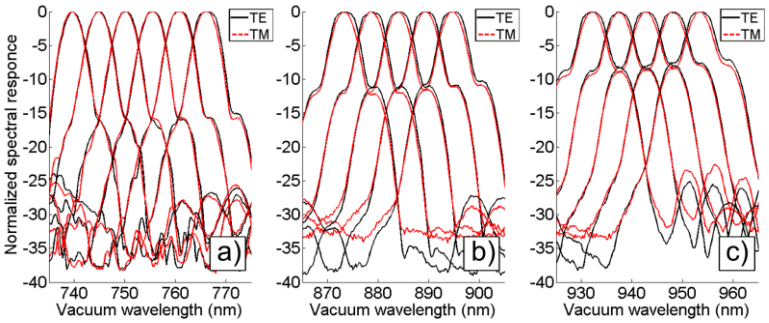

Fig. 10. (Color online) Normalized spectral response of the AWG measured for both, TE and TM polarizations, and for three different spectral regions: a) 740–770 nm; b) 870–900 nm; c) 930–960 nm.

In Figs. 9 and 10 we observe that for all the output channels of the AWG two shoulders are present next to the main peak. We also observe that the intensity of the shoulders increases with wavelength. The shoulders can also be observed, although with lower intensity, in the 2D beam-propagation-method (BPM) simulation shown in Fig. 11(a). The simulation is phase error free, so the shoulders are not caused by phase errors in the design.

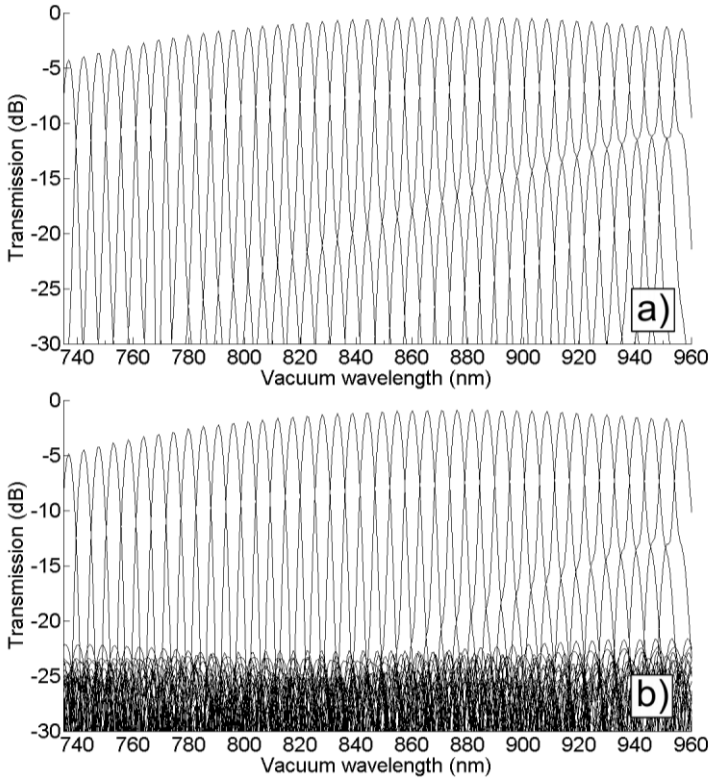

Fig. 11. (a) Simulated spectral response for TE polarization using the 2D beam-propagation-method (BPM) with no phase errors, (b) with random phase errors distributed between 0 and 80 degree.

We attribute the shoulders to coupling between the output-channels of the AWG which are initially spaced by 6 μm and then separate from each other at an angle of ~0.086 degrees. The

#142949 - $15.00 USD Received 18 Feb 2011; revised 15 Apr 2011; accepted 17 Apr 2011; published 20 Apr 2011

small separation distance was chosen in the design phase as a compromise between increased crosstalk due to coupling and reduced size of the device and therefore lower propagation losses. We preferred low losses and higher crosstalk since for our target application (Raman sensing) low losses are a must while there are no stringent specifications on the crosstalk. We also performed 2D BPM simulations (see Fig. 11(b)) adding random phase errors (distributed in the interval 0 – 80 degrees) in all the arrayed waveguides, to show how the effect of these errors increases the noisy background to around −25 dB, which is similar to what we observe in the measurement.

The fabricated device has dimensions of 5 cm by 2 cm, occupying a large area on the wafer, and for this reason the variations in the material properties and layer thickness across the wafer cause phase errors. These can be seen by comparing Fig. 9 and Fig. 11. We notice that the peak width in the fabricated device is larger than in the simulations, and that there is a small shift in the central wavelengths of the external channels with respect to the simulated values. The presence of these fabrication-related phase errors does not enable us to demonstrate the cancellation of the systematic phase errors arising from the use of different bends in the fabricated device.

5. Conclusions

We have presented a detailed description of a novel layout for the design of AWGs of any diffraction order. The proposed layout makes use of identical bends across the entire grating, leading to a complete cancellation of systematic phase errors which are intrinsically present in conventional designs. We have shown that our layout occupies a smaller area than the conventional horse-shoe layout and, through simulations, that our layout allows us to reduce the device size more than it would be possible with a conventional design without incurring a significant distortion of the AWG response due to the increase of the systematic phase errors at smaller bending radii. Furthermore, we have designed, fabricated, and characterized a broadband AWG according to the proposed layout and demonstrated low losses and polarization insensitivity of the device over a wide spectral range of 215 nm in the near-infrared spectral region.

Appendix

In this appendix we describe the design of a generic AWG according to our proposed geometry. The procedure does not lead to a single unique design, as it involves a number of arbitrary choices, some of which are restricted by the available waveguide fabrication technology. Other restrictions arise from topological feasibility requirements: waveguides should be laid out in such a way that they are everywhere sufficiently separated from each other and do not intersect with each other. We introduce the design equations, which will need to be solved iteratively.

The design starts from the initial specifications (central wavelength, wavelength resolution, FSR, waveguide geometry, etc.), from which a number of parameters is determined by use of the AWG design equations [9], such as the length R of the FPR, the arrayed-waveguide spacing d at the FPR, the order m of the AWG, the number of arrayed waveguides N, the length difference ΔL, and the tilt $\Delta\alpha$ between adjacent waveguides. The minimum bending radius $r_{\min}$ that leads to acceptable bend losses is determined once the geometry of the waveguides is known. At this point the bend of type 2 can be designed, while the design of the bend of type 1 is related to the angle α and must be approached in an iterative way, as discussed later. Our design depends loosely on the bend choice, since the only bend parameter that enters the design is the chord of the bend P (see Fig. 3) for the bend of type 1, and equivalently ΔP (not shown) for type 2.

Our AWG layout is not anti-symmetric. The two halves of the AWG are different and need to be designed in separate steps. We commence with designing the left half:

#142949 - $15.00 USD Received 18 Feb 2011; revised 15 Apr 2011; accepted 17 Apr 2011; published 20 Apr 2011

1. We arbitrarily choose initial values for the constant a, the waveguide separation s on the line $\overline{\mathrm{AB}}$, the angle α, and the lengths of the straight sections l_{p1} and l_{q1} of the first waveguide (our reference waveguide).
2. Once α is determined, we choose the bend of type 1 and, therefore, the value of P.
3. From simple geometrical relations we find D and H (see Fig. 3).
4. For each waveguide of the left half (i = 2, 3, …, N), we determine the lengths of the three straight sections l_{pi}, l_{qi}, and l_{ri}.

Step 4 is performed analytically by solving a system of three equations, which is found in the following way. The i^{th} waveguide has one bend of type 1 and $i - 1$ bends of type 2 (dotted line in the figure) of length $l_{\Delta\alpha}$. The lengths of the waveguides belonging to the left half can be expressed as:

$$\begin{aligned} l_1 &= R + l_{p1} + l_\alpha + l_{q1} \\ l_2 &= R + l_{p2} + l_\alpha + l_{q2} + l_{\Delta\alpha} + l_{r2} \\ &\ldots \\ l_i &= R + l_{pi} + l_\alpha + l_{qi} + (i-1)l_{\Delta\alpha} + l_{ri} \\ &\ldots \end{aligned} \tag{1}$$

Recalling that the length difference between two adjacent waveguides on the left half is given by $a + \Delta L/2$, we find a first equation by expressing the length difference between the i^{th} waveguide and the reference waveguide as $(i - 1)$ $(a + \Delta L/2)$:

$$l_{pi} + l_{qi} + l_{ri} = (i-1)\left(a + \frac{\Delta L}{2}\right) + l_{p1} + l_{q1} - (i-1)l_{\Delta\alpha}. \tag{2}$$

Two other equations can be derived from the requirements that the connection points of the waveguides are all on the line $\overline{\mathrm{AB}}$ and that these end points should be equidistant with a given spacing s. These equations read:

$$\begin{aligned} &(R + l_{pi})\cos\left(\alpha + (i-1)\Delta\alpha\right) + P\cos\left(\alpha/2 + (i-1)\Delta\alpha\right) + .. \\ &\quad + l_{qi}\cos\left((i-1)\Delta\alpha\right) + \sum_{j=1}^{i-1}\Delta P\cos\left((i-1-j/2)\Delta\alpha\right) + l_{ri} = D, \end{aligned} \tag{3}$$

$$\begin{aligned} &(R + l_{pi})\sin\left(\alpha + (i-1)\Delta\alpha\right) + P\sin\left(\alpha/2 + (i-1)\Delta\alpha\right) + .. \\ &\quad + l_{qi}\sin\left((i-1)\Delta\alpha\right) + \sum_{j=1}^{i-1}\Delta P\sin\left((i-1-j/2)\Delta\alpha\right) = H + (i-1)s = H_i. \end{aligned} \tag{4}$$

For each variation of α the steps 2, 3, and 4 need to be performed. By plotting the solutions of Eqs. (2)–(4) as a function of α, we find the range of angles α for which all three lengths are non-negative. The angle α must be between 0 and $\pi/2$ (an initial choice could be $\pi/4$; the optimum value of α leads to the smallest footprint of the left half). If no value of α exists for which this condition is satisfied, the initial parameters a, s, l_{p1}, and l_{q1} have to be adjusted. The procedure requires solving N linear systems of three equations for three unknowns. The separation s between the arrayed waveguides on line must guarantee that there is negligible coupling between the arrayed waveguides at the point where adjacent waveguides are closest to each other. Since the arrayed waveguides are tapered as they approach the FPR region, l_{p1} should be 2 or 3 times the taper length. A large value (2 or 3 times l_{p1}) must be chosen for l_{q1}.

For the design of the right half, see Fig. 3(b), of the AWG a similar procedure has to be applied:

#142949 - $15.00 USD Received 18 Feb 2011; revised 15 Apr 2011; accepted 17 Apr 2011; published 20 Apr 2011

1. To determine the lengths of the straight sections l'_{pN} and l'_{qN} of the topmost waveguide (the reference waveguide with number N), we impose two conditions -arbitrary to a degree- intended to make this second half of the AWG of similar size as the first half. The first condition sets the length of this waveguide,

$$l'_N = R + l'_{pN} + l_\alpha + l'_{qN} = l_1 + (N-1)\Delta L/2, \tag{5}$$

while the second condition is that $H' = H$, which yields

$$R\sin(\alpha) + l'_{pN}\sin(\alpha) + P\sin(\alpha/2) = H \tag{6}$$

It is straightforward to solve this set of equations, as R, l_1, l_α, N, ΔL, α, P, and H have been determined before.

2. Subsequently, we find the value of D' (which is different from D) and then proceed, as before, by determining for each waveguide of the right half ($i = N - 1, N - 2, \ldots, 1$) the lengths of the three straight sections l'_{pi}, l'_{qi}, and l'_{ri}.

Our choice of imposing similar footprints makes it more likely that, with a certain choice of initial parameters, meaningful solutions are found for both halves of the AWG, thereby reducing the iteration steps necessary to design the geometry.

Acknowledgment

The authors acknowledge financial support from the IOP Photonic Devices supported by the Dutch funding agencies NLAgency and STW.

#142949 - $15.00 USD Received 18 Feb 2011; revised 15 Apr 2011; accepted 17 Apr 2011; published 20 Apr 2011